Contributions of GCM/RCM Uncertainty in Ensemble Dynamical Downscaling for Precipitation in East Asian Summer Monsoon Season

Asuka Suzuki-Parker[1], Hiroyuki Kusaka[1], Izuru Takayabu[2],
Koji Dairaku[3], Noriko N. Ishizaki[1], and Suryun Ham[4]
[1]*University of Tsukuba, Tsukuba, Ibaraki, Japan*
[2]*Meteorological Research Institute, Tsukuba, Ibaraki, Japan*
[3]*National Research Institute for Earth Science and Disaster Resilience, Tsukuba, Ibaraki, Japan*
[4]*APEC Climate Center, Busan, the Republic of Korea*

Abstract

Targeting to East Asian summer monsoon for the first time, this study presents an assessment of projection uncertainty in ensemble dynamical downscaling (DDS) simulations. Based on 12-member DDS simulations comprised of three global climate models (GCMs) and four regional climate models (RCMs), we evaluate contributions of GCM and RCM uncertainty to the total uncertainty of summer-time precipitation projections around Japan.

Our results show that contribution of RCM uncertainty can be comparable to that of GCM uncertainty in magnitudes. This finding draws a distinction from the past studies showing the dominance of GCM uncertainty. Most notably, our results show that RCM uncertainty for number of precipitating days appears around and over the land. RCM uncertainty for precipitation amounts also shows a dependence on topography but to a lessor degree. These RCM uncertainty characteristics are potentially linked to the difference in various RCM configurations such as physics schemes and model topography. In contrast, GCM uncertainty mostly appears over the ocean, which can be attributed to the difference in the GCM's future projections of East Asian summer monsoon. Our finding may be of an importance for water disaster and water resource management with DDS.

(**Citation**: Suzuki-Parker, A., H. Kusaka, I. Takayabu, K. Dairaku, N. N. Ishizaki, and S. Ham, 2018: Contributions of GCM/RCM uncertainty in ensemble dynamical downscaling for precipitation in East Asian summer monsoon season. *SOLA*, **14**, 97−104, doi:10.2151/sola.2018-017.)

1. Introduction

Dynamical downscaling (DDS) provides essential information for adaptation strategies for climate change. The increasing social need for fine-scale climate change information have promoted internationally coordinated DDS projects, such as the ENSEMBLES project (van der Linden and Mitchell 2009), the NARCCAP project (Mearns et al. 2012), and the CORDEX project. These projects employ multiple global circulation models (GCMs) and regional climate models (RCMs) to construct ensemble projections. However, how best to select GCMs and RCMs for efficient sampling of projection uncertainty is not yet certain (e.g., Rummukainen et al. 2015; Takayabu et al. 2016).

Motivated by this challenge, studies have assessed contributions of GCM and RCM uncertainty to the total projection uncertainty in the PRUDENCE and the ENSEMBLES simulations (Rowell 2005; Déqué et al. 2007; Déqué et al. 2012). Their results indicated that GCM uncertainty was generally larger than RCM uncertainty. However, these studies did not directly evaluate GCM and RCM uncertainty because not all RCMs were downscaled from all GCMs. Moreover, their results were based on DDS simulations for Europe only. Assessments for various climate zones are necessary considering the on-going efforts for coordinated DDS simulations throughout the world.

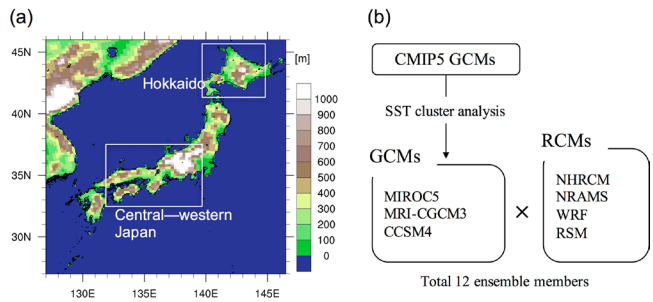

Fig. 1. (a) Map of topography for analysis region, and (b) schematic illustration of the multi GCM/RCM dynamical downscaling ensemble simulation design.

East Asia is no exception in this regard. Among many DDS simulations conducted for this area, those targeting Japan have shown that downscaled precipitation patterns vary by RCMs (Iizumi et al. 2011; Ishizaki et al. 2012; Tsunematsu et al. 2013). At the same time, as future projections of East Asian monsoon vary by GCMs (e.g., Kitoh and Uchiyama 2006), it is important to assess both GCM and RCM uncertainty in DDS simulations. Inatsu et al. (2015) assessed projection uncertainties in multi-GCM × multi-RCM DDS simulations and showed that GCM uncertainty was generally larger than RCM uncertainty. However, their results do not represent the whole Japan as the study region (Hokkaido, Fig. 1a) is not under the influence of East Asian summer monsoon.

This study performs multi-GCM × multi-RCM DDS simulations around Japan to evaluate contributions of GCM and RCM uncertainty to the total uncertainty of summer-time (June-August, JJA) precipitation projection. Bearing in mind of impact assessments for drought and extreme rainfall, we evaluate three precipitation related variables; total precipitation amount, number of precipitating days, and extreme precipitation. The DDS simulations comprises of four RCMs each downscaled from three GCMs, enabling direct assessment of uncertainty without arbitrarily filling "missing DDS members".

2. Ensemble DDS simulation design

The ensemble DDS simulations analyzed in the present study consist of four RCMs and three GCMs, with a total of 12 ensemble members (Fig. 1b). Model simulations are 20-years each for current (1981−2000) and future climates (2081−2100). The RCP4.5 scenario (IPCC 2013) is used for the future climate simulation.

The four RCMs used for downscaling are NHRCM (Saito

Corresponding author: Asuka Suzuki-Parker, Faculty of Geo-environmental Sciences, Rissho University, 1700 Magechi, Kumagaya, Saitama 360-0194, Japan. Email: suzukiparker@ris.ac.jp.

©The Author(s) 2018. This is an open access article published by the Meteorological Society of Japan under a Creative Commons Attribution 4.0 International (CC BY 4.0) license (http://creativecommons.org/license/by/4.0).

et al. 2006), NRAMS (Pielke et al. 1992), WRF (Skamarock et al. 2008), and RSM (Juang 2000). These RCMs are selected based on their extensive applications around Japan (Iizumi et al. 2011; Ishizaki et al. 2012; Ham et al. 2016; Kusaka et al. 2016; Nayak and Dairaku 2016; Nayak et al. 2017). The horizontal resolution is commonly set at 20 km with the model domain covering the Japanese islands and the surrounding vicinity (Fig. 1a). However, number of grid points (and thus lateral boundary locations) and physics scheme selections are different by RCMs (Table A1). Additionally, dynamical cores are varied as the RSM is a spectral model while the other three RCMs are finite volume difference models. Finally, representations of topography in the RCMs also show variation (discussed in Section 4.3). Therefore, RCM uncertainty assessed in this study includes comprehensive impacts from differences in dynamical core types, domain configurations, physics schemes, and model topography.

The three GCMs used as initial and boundary conditions for the RCMs are MIROC5, MRI-CGCM3, and CCSM4. These GCMs are selected bearing in mind that future projections of precipitation patterns in monsoon regions are sensitive to future changes in tropical sea surface temperatures (SST) (i.e., Xie et al. 2010). Specifically, GCMs in the Coupled Model Intercomparison Project Phase 5 were categorized into three groups according to their future tropical SST projections by cluster analysis (the work by Mizuta et al. 2014), then, the GCMs are selected from each of the three groups. Original 6-hourly GCM output data are used as initial and boundary conditions for the RCMs. Neither bias correction nor spectral nudging is applied.

3. Current climate reproducibility

Prior to the assessment of future projection, we briefly survey reproducibility of the simulated precipitation pattern for current climate. Figure 2 shows the simulated current climate JJA mean precipitation from each of the DDS ensemble members along with the Automated Meteorological Data Acquisition System (AMeDAS) observation data.

Synoptic scale band-shaped precipitation associated with East Asian summer monsoon (hereafter referred to as Baiu rain band, also called Mei-yu in China and Changma in Korea) is well captured by all members. Locations of Baiu rain band differ by GCMs; those downscaled from MRI-CGCM3 and CCSM4 produced the rain band along the southern shore on the Pacific side of western Japan (Figs. 2e, 2f, 2g, 2h, 2i, 2j, 2k, and 2l), but those downscaled from MIROC5 produced the rain band off-shore on the south of the Japanese archipelago (Figs. 2a, 2b, 2c, and 2d).

Localized heavy precipitation due to topography are also well reproduced by all members (Figs. 2a, 2b, 2c, 2d, 2e, 2f, 2g, 2h, 2i, 2j, 2k, and 2l). Qualitative evaluations of the DDS results are shown in Fig. A1. The AMeDAS is selected as the basis of evaluation because of its high density observation network (located at 17 km intervals on average). Taylor skill scores (TSS, Taylor 2001) vary by RCMs rather than by GCMs, as the variances of TSS among RCM and GCM are 0.017 and 0.002, respectively. Bias and root mean square error show variations by RCMs (e.g., NHRCM simulations have high root mean square errors) but also show variations by GCMs (e.g, members downscaled from MRI-CGCM3 tend to have low bias) (Fig. A1b).

The main question for this study is whether or not these variations in current climate simulations persist in the future projections.

4. Uncertainty assessment for future projection

4.1 Quantifying sources of uncertainty by two-way analysis of variance with replication

There are three distinct sources of uncertainty in climate change projections; scenario uncertainty, model uncertainty, and interannual (natural) variability (e.g., Hawkins and Sutton 2011). In DDS, model uncertainty incorporates RCM uncertainty and GCM uncertainty. We also expect to have uncertainty due to interactions between RCM and GCM. This is hereafter referred to as interactive effect.

We use variance as a measure of uncertainty. The total variance among the 12 members is decomposed to variances by RCM, GCM, interactive effect, and the residual, using two-way analysis of variance (ANOVA) with replication (von Storch and Zwiers 1999) as follows.

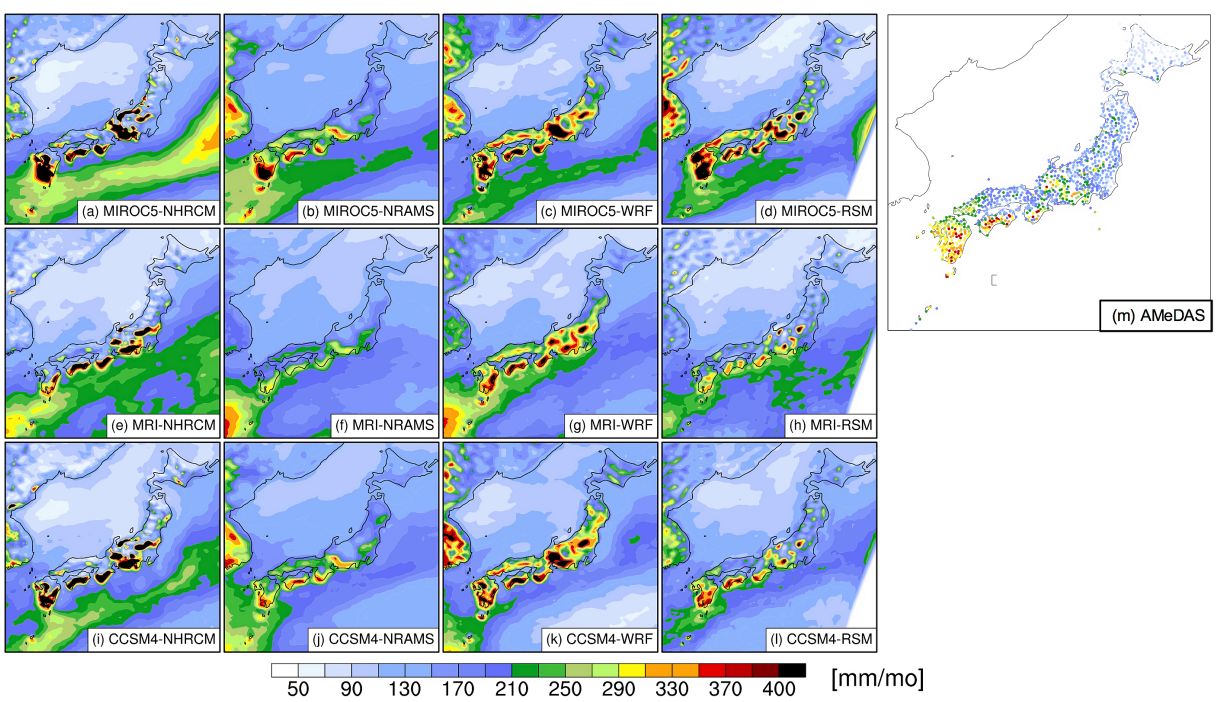

Fig. 2. Monthly mean precipitation amount averaged for June−August 1981−2000 from (a−l) the ensemble DDS simulations, and (m) the AMeDAS observations.

$$
\begin{aligned}
var_{tot} &= var_{GCM} + var_{RCM} + var_{GCM\times RCM} + \varepsilon \\
&= \frac{1}{3}\sum_{g=1}^{3}\left(\overline{x_{g**}} - \overline{x_{***}}\right)^2 + \frac{1}{4}\sum_{r=1}^{4}\left(\overline{x_{*r*}} - \overline{x_{***}}\right)^2 \\
&\quad + \frac{1}{3\times 4}\sum_{g=1}^{3}\sum_{r=1}^{4}\left(\overline{x_{gr*}} - \overline{x_{g**}} - \overline{x_{*r*}} + \overline{x_{***}}\right)^2 \\
&\quad + \frac{1}{3\times 4\times 20}\sum_{g=1}^{3}\sum_{r=1}^{4}\sum_{y=1}^{20}\left(x_{gry} - \overline{x_{gr*}}\right)^2 \qquad (1)
\end{aligned}
$$

Here, x_{gry} denotes DDS result from RCM (r) downscaled from GCM (g) for year (y). The over bar denotes average, and the subscript (*) indicates 'all' so for example, $\overline{x_{g**}}$ is the all-year (20 years) average of all RCMs (four RCMs) downscaled from one (common) GCM. Mathematically, the residual term corresponds to interannual variability. We perform ANOVA to future changes of JJA precipitation amount (PR), number of precipitation day (PR_day), and extreme precipitation (PR95). PR_day is defined as number of days with daily precipitation exceeding 0.1 mm, and PR95 is defined as 95th percentile value of JJA daily precipitation amount including 0 mm/day (e.g., daily precipitation amount on non-precipitating days). Note that we are unable to quantify scenario uncertainty as the 12-member DDS simulations analyzed in this study target single scenario (RCP4.5 scenario).

The results are presented in Fig. 3 as fractions of uncertainty explained by RCM, GCM and interactive effect, to the total projection uncertainty. Only statistically significant fractions (with $p < 0.05$) are shown. Note that the fractions are small (less than ~0.1) as the residual (4th term in Eq. 1) is very large. This indicates that most (up to 90%) of the total variance is explained by the residual, which corresponds to interannual variability. Further discussion on this topic will be given in Section 5.

There are three major findings in Fig. 3.

(1) RCM uncertainty, GCM uncertainty, and interactive effect all have statistically significant contributions to the total projection uncertainty.
(2) Contribution of RCM uncertainty can be comparable to that of GCM uncertainty in magnitudes.
(3) Appearance of RCM and GCM uncertainty varies in space. Specifically, GCM uncertainty tends to appear cohesively over the ocean, while RCM uncertainty is less cohesive and tend to appear more over and around the land.

The following subsections present detailed descriptions of each uncertainty factors and their possible causes.

4.2 GCM uncertainty

As mentioned above, most of GCM uncertainty is observed over the ocean, but its spatial patterns vary by variables (Figs. 3a, 3d, and 3g). For PR, GCM uncertainty is observed in north

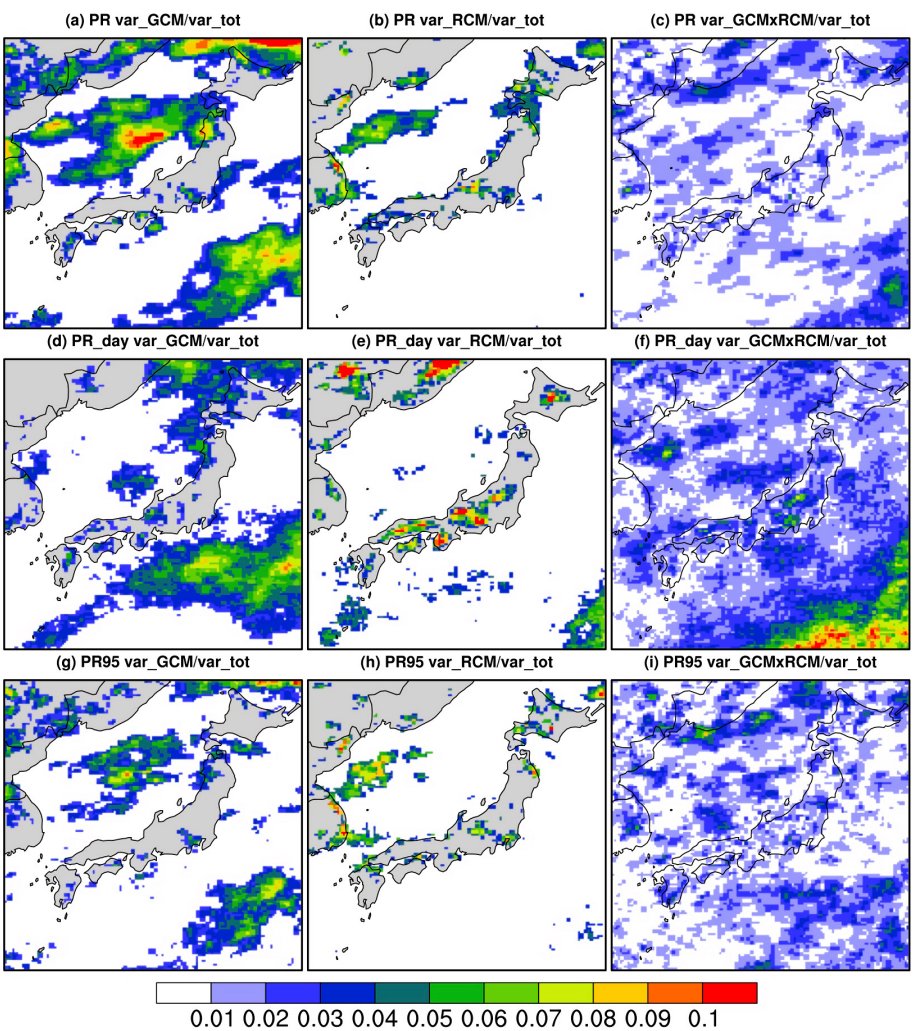

Fig. 3. Fractions of variance explained by GCM difference (panels in left columns), RCM difference (middle column), and interactive effect between GCM and RCM differences (right column) for future changes of PR (top row), PR_day (middle row), and PR95 (bottom row) as simulated by the ensemble DDS simulations. Only areas with statistical significance ($p < 0.05$) are plotted. Note that fractions are small (less than ~0.1) as the residual (4th term in Eq. 1, corresponding to interannual variability) is very large.

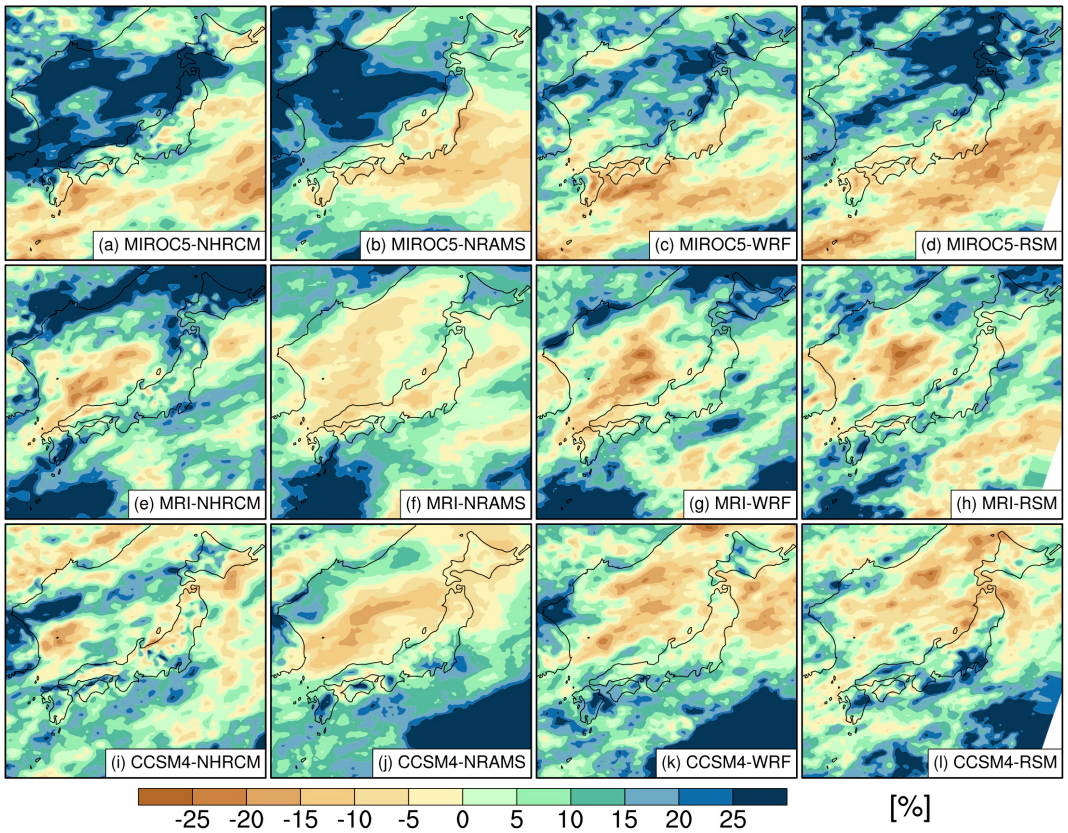

Fig. 4. Future changes in JJA PR between current climate (1981−2000) and future climate (2081−2100, under RCP4.5 scenario) as projected by the ensemble DDS simulations.

of Hokkaido, in the Sea of Japan, and in the Pacific Ocean on the southeast of Japan (Fig. 3a). Similar pattern is observed for PR95, but with smaller magnitudes (Fig. 3g). For RP_day, GCM uncertainty is observed in the Pacific on south of Japan but is less apparent in the Sea of Japan (Fig. 3d).

In order to investigate possible causes for GCM uncertainty in PR, we examine future changes of PR projected by the individual DDS members (Fig. 4). In general, members downscaled from MIROC5 show reductions in southern Japan and increases in northern Japan (Figs. 4a, 4b, 4c, and 4d). This pattern implies precipitation reductions along the Baiu rain band. On the other hand, members downscaled from CCSM4 show opposite patterns: Increases in southern Japan and reductions in northern Japan (Figs. 4i, 4j, 4k, and 4l). This pattern implies precipitation increases along the Baiu rain band. Members downscaled from MRI-CGCM3 show reductions in the Sea of Japan, but the rest of regions show mixed results by members. Future changes of PR95 also show similar GCM dependency, with precipitation reductions along the Baiu rain band in members downscaled by MIROC5 (Figs. A2a, A2b, A2c, and A2d) and the opposite in members downscaled by CCSM4 (Figs. A2i, A2j, A2k, and A2l). Projections of PR_day by individual DDS members also show marked GCM dependency, especially around Hokkaido and in the Pacific Ocean south of Japan (Fig. 5).

These GCM dependency can be attributed to different projections of East Asian summer monsoon in the forcing GCMs, which is illustrated in Fig. 6. MIROC5 projects southwesterly anomalies at 850 hPa and higher increase of moisture around Japan (Fig. 6b), resulting in a northward shift of monsoonal flow and precipitation increase in Sea of Japan (Fig. 6a). On the other hand, MRI-CGCM3 and CCSM4 show westerly anomalies around Japan with less moisture increase (Figs. 6d and 6f), leading to precipitation reductions in the Sea of Japan and increases in the Pacific side of Japan for both GCMs (Figs. 6c and 6e). Precipitation changes associated with the East Asian summer monsoon are generally more apparent over the ocean than on land (Fig. 4). Therefore, GCM uncertainty appearing over the ocean is considered to be due to the difference in the GCM's projections of East Asian summer monsoon.

4.3 RCM uncertainty

RCM uncertainty is due to differences in various aspects of RCMs, such as dynamics, physics schemes, model domain configurations (including map projections, locations of lateral boundaries, vertical coordinates, etc) and model topography. Isolation of the impact caused by each of these aspects is not possible in the present study. However, some discussions on the possible causes can be deduced based on the observed characteristics of RCM uncertainty shown in Fig. 3.

For PR and PR95, high RCM uncertainty is observed in west side of the Sea of Japan (Figs. 3b and 3h). This is due to difference in the magnitude of projected changes among RCMs shown in Figs. 4 and A2. For example, among the members downscaled from CCSM4, WRF and RSM show greater reductions compared to NHRCM and NRAMS in this area (Figs. 4i and 4j). Projections for PR95 are also similar (Figs. A2i and A2j). This implies that while forcing GCMs control the sign (plus or minus) of the change, differences in RCMs influence the magnitude of the change. This may be related to differences in model domain configurations and/or physics schemes in RCMs (see Table A1). Another potential cause is the difference of western lateral boundary locations, which can alter moisture influx from monsoon flow into the RCM domains. Outside of the Sea of Japan, RCM uncertainty is observed on the land and along the coastlines (Figs. 3b and 3h). This may be due to the interactions between RCM differences listed in Table A1 and the differences in land/sea boarder locations and model topography.

Compared to PR and PR95, RCM uncertainty for PR_day is

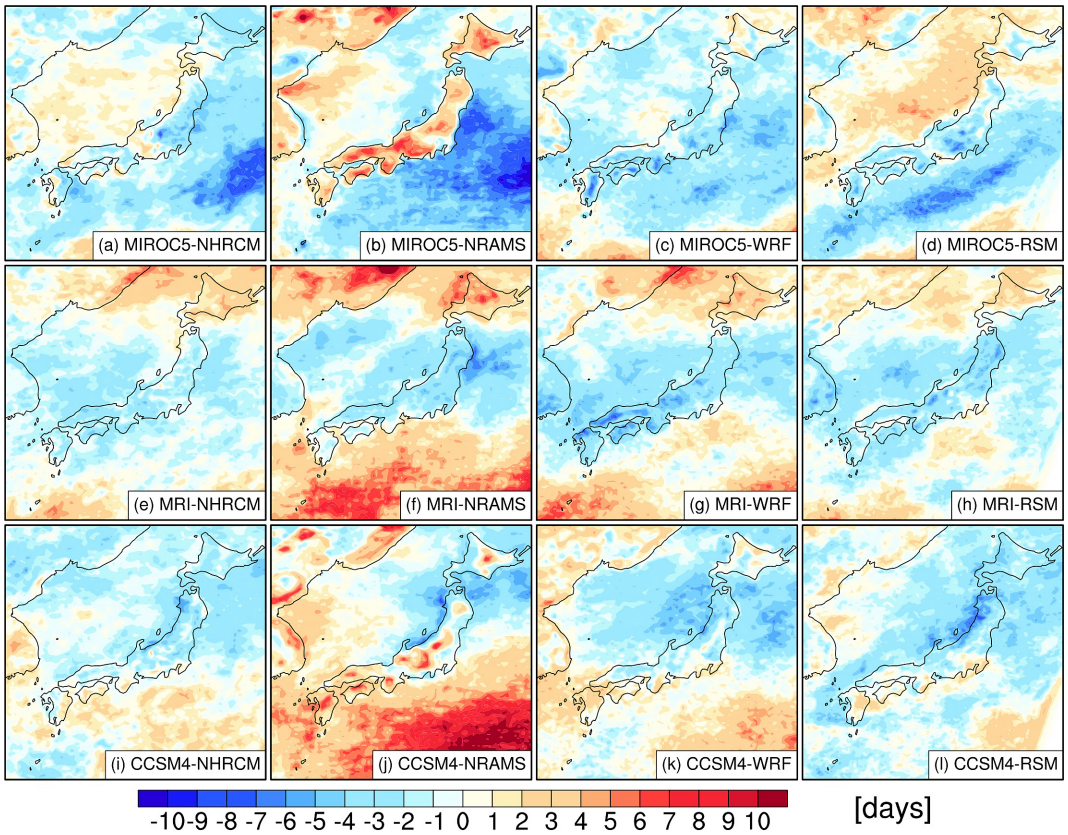

Fig. 5. Similar to Fig. 4, but for PR_day.

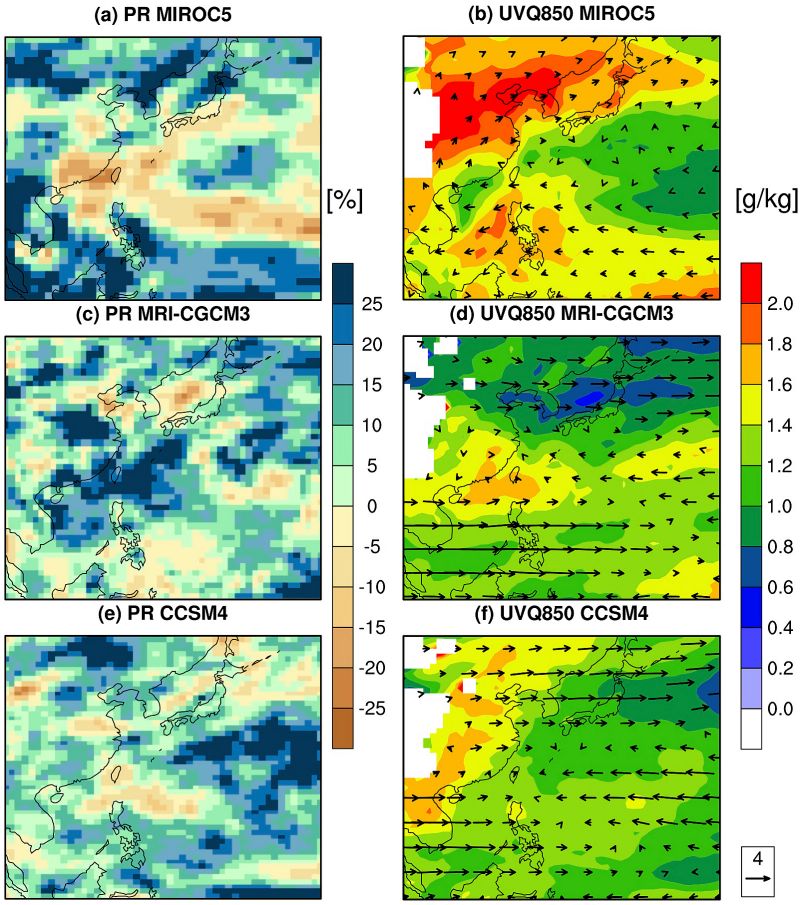

Fig. 6. Future changes of JJA PR (left column), and 850 hPa winds and specific humidity (right column) from the MIROC5 (top row), the MRI-CGCM3 (middle row), and the CCSM4 (bottom row). In the panels on the right column, colored contours show specific humidity [g/kg] and vectors show winds [m/s] (legend shown on the bottom right corner of the figure).

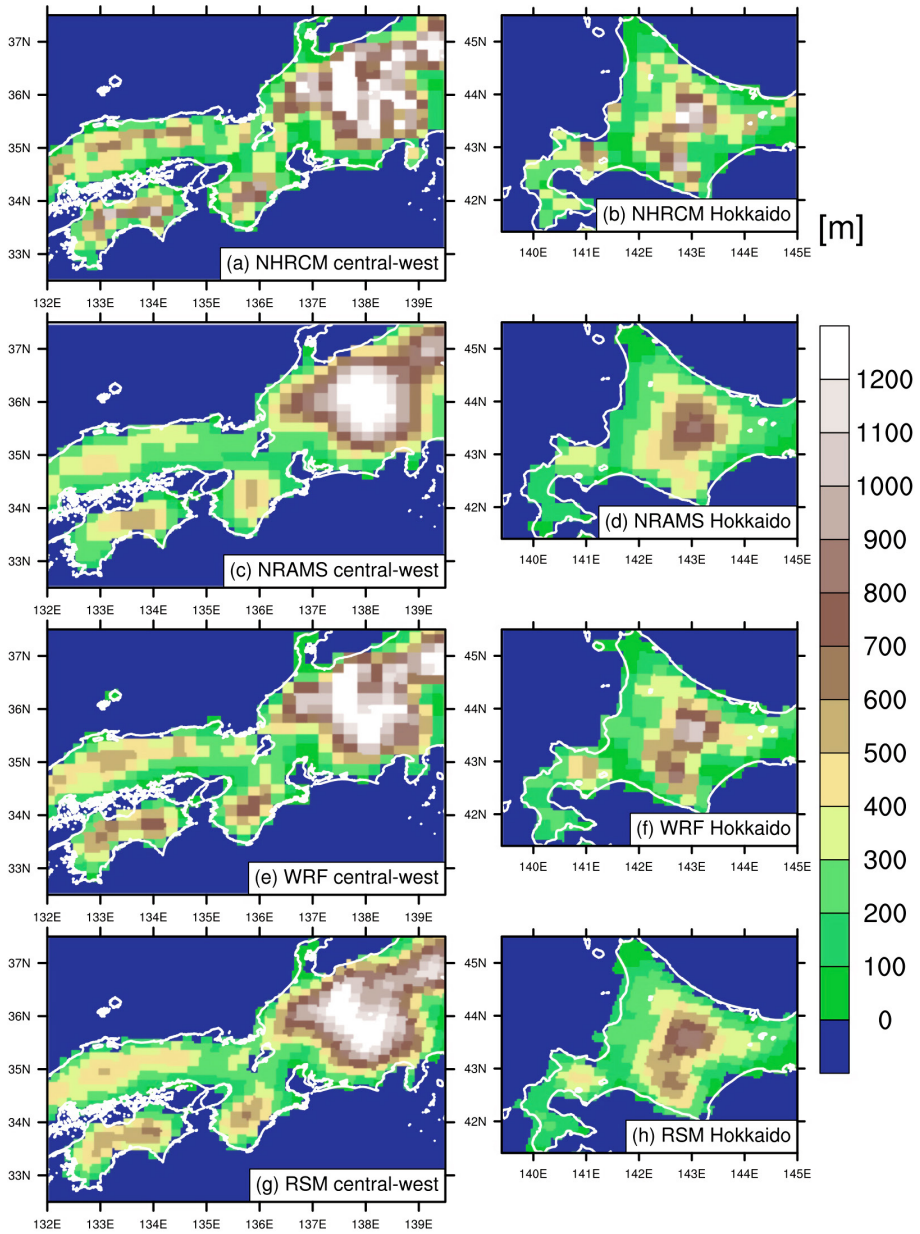

Fig. 7. Model topography for central~western Japan and Hokkaido (areas enclosed by white boxes in Fig. 1a) from (a−b) NHRCM, (c−d) NRAMS, (e−f) WRF, and (g−h) RSM.

higher and tends to appear more over the lands (Fig. 3e). Most notably, localized areas of high uncertainty are observed in mountainous regions. One of the possible causes here is the distinctive projections of NRAMS (Fig. 5). In fact, RCM uncertainty becomes statistically insignificant if NRAMS simulations are removed from the ensemble. It is likely that NRAMS's distinctive projections are related to its smooth model topography (Fig. 7). It is noteworthy that PR_day projection is seemingly sensitive to model topography while PR an PR95 do not show apparent sensitivity. This may be related to the different nature of these variables: PR and PR95 are based on precipitation amounts, whereas PR_day is threshold-sensitive and has a binary aspect (e.g., presence or absence of daily precipitation). We also note that PR_day may be resolution-sensitive as recently shown by Sugimoto et al. (2018).

4.4 Interactive effect

Fractions of uncertainty explained by interactive effect are smaller compared to GCM and RCM uncertainty, amounting only up to a few percent of the total projection uncertainty (Figs. 3c, 3f, and 3j). Uncertainty by interactive effect is scattered randomly in space except for over the ocean southeast of Japan where it shows a relatively cohesive pattern. Compared to PR and PR95, PR_day has larger uncertainty by interactive effect overall. This may be related to the aforementioned characteristics of RCM uncertainty, where PR_day has higher RCM uncertainty compared to PR and PR95.

5. Concluding remarks

For the first time in East Asian summer monsoon, the present study directly evaluated contributions of GCM and RCM uncertainty to the total projection uncertainty of JJA precipitation in multi-GCM/RCM DDS simulations around Japan. The analysis was based on 12-member DDS simulations comprised of four

RCMs (NHRCM, NRAMS, WRF, RSM) each downscaled from three GCMs (MIROC5, MRI-CGCM3, CCSM4). Current and future climates each targeted for 1981−2000, and 2081−2100 under the RCP4.5 scenario, respectively.

A brief evaluation of the current climate reproducibility showed that all DDS members reproduced a synoptic-scale band of precipitation associated with the Baiu rain band. Localized areas of heavy precipitation associated with topography were also well captured.

The results showed that GCM uncertainty, RCM uncertainty, and their interactive effect all have statistically significant contributions to the total projection uncertainty of PR, PR_day, and PR95. Their contributions varied by locations and variables. Specifically, GCM uncertainty was most significant over the ocean, whereas RCM uncertainty for PR_day was significant around and over the land. RCM uncertainties for PR and PR95 were significant over the land but signals were also observed over the ocean. GCM uncertainty was associated with differences in projected future changes of the Baiu rain band in the forcing GCMs. Potential causes for RCM uncertainty may include differences in physics schemes and model topography in RCMs, but further deduction was not possible in this study. Appearance of the interactive effect was spatially random and relatively small.

In general, GCM uncertainty is considered to be the dominant source of uncertainty in multi-GCM/RCM DDS simulations (Rowell 2005; Déqué et al. 2007; Déqué et al. 2012; Inatsu et al. 2015). Our findings draw a distinction from the past studies in the following two aspects. First, contribution of RCM uncertainty can be comparable to that of GCM uncertainty in magnitudes, depending on the area and variable of interest. Second, RCM uncertainty tend to appear around and over the land, and its characteristics differ for precipitation amount and number of precipitating days. The latter point calls for an attention in the social impact assessment such as water disaster and water resource management.

Another important finding from our analysis is that RCM uncertainty, GCM uncertainty, and their interactive effect contribute to only less than 10% of the total projection uncertainty. The rest is attributed to the residual, which corresponds to interannual variability amounting up to 90% of the total projection uncertainty. This finding is clearly different from Hawkins and Sutton (2011), who showed that interannual variability had small (less than 30%) contribution to uncertainty in the precipitation projection for the end of 21st century. The probable reason for this difference is that our analysis targeted regional changes around Japan using DDS, whereas Hawkins and Sutton examined at a broader scale using GCMs. Our results highlight the importance of the projection uncertainty assessment at various spatio-temporal scales with different projection approaches.

Acknowledgements

Forcing GCM data were prepared by Mr. Osamu Arakawa (JAMSTEC), Dr. Hidetaka Sasaki (MRI), and Dr. Masahiro Watanabe (University of Tokyo). The authors extend sincere thanks to Mr. Toshiharu Nagatomo for data management. This work was conducted under the framework of the SOUSEI/TOUGOU programs of the MEXT, Japan. Parts of the DDS simulations were performed using COMA at the CCS, University of Tsukuba.

Edited by: H. Fudeyasu

Supplement

Table A1: Specifications of the RCMs.

Figure A1: (a) Taylor diagram (Taylor 2001) and (b) scatter plot of bias and root-mean square error (RMSE) for current climate simulations (1981−2000) JJA PR. Validation data is AMeDAS observation.

Figure A2: Similar to Fig. 4, but for 95th percentile value of JJA daily precipitation.

References

Chen, C., and W. R. Cotton, 1983: A one-dimensional simulation of the stratocumulus-capped mixed layer. *Bound.-Layer Meteor.*, **25**, 289−321.

Chen, D.-X, and M. B. Coughenour, 1994: GEMTM: A general model for energy and mass transfer of land surfaces and its application at the FIFE sites. *Agri. Forest Meteor.*, **68**, 145−171.

Chen, F., and J. Dudhia, 2001: Coupling an advanced land-surface hydrology model with the Penn State/NCAR MM5 modeling system. Part I: Model implementation and sensitivity. *Mon. Wea. Rev.*, **129**, 569−585.

Chou, M.-D., 1992: A solar radiation model for use in climate studies. *J. Atmos. Sci.*, **49**, 762−772.

Chou, M.-D., K.-T. Lee, S.-C. Tsay, and Q. Fu, 1999: Parameterization for cloud longwave scattering for use in atmospheric models. *J. Climate*, **12**, 159−169.

Déqué, M., D. P. Rowell, D. Lüthi, F. Giorgi, J. H. Christensen, B. Rockel, D. Jacob, E. Kjellström, M. de Castro, and B. van den Hurk, 2007: An intercomparison of regional climate simulations for Europe: Assessing uncertainties in model projections. *Climatic Change*, **81**, 53−70.

Déqué, M., S. Somot, E. Sanchez-Gomez, C. M. Goodess, D. Jacob, G. Lenderink, and O. B. Christensen, 2012: The spread amongst ENSEMBLES regional scenarios: Regional climate models, driving general circulation models and interannual variability. *Climate Dyn.*, **38**, 951−964.

Eito, H., M. Yoshizaki, T. Kato, K. Saito, and Y. Mano, 1999: 3-D numerical experiments of marine stratocumulus observed around Japan islands in winter. *CAS/JSC WGNE Res. Activ. Atmos. Oceanic Modell.*, **28**, 5.21−5.22.

Ek, M. B., K. E. Mitchell, Y. Lin, E. Rogers, P. Grunmann, V. Koren, G. Gayno, and J. D. Tarpley, 2003: Implementation of Noah land surface model advances in the National Centers for Environmental Prediction operational mesoscale Eta model. *J. Geophys. Res.*, **108**, 8851, doi:10.1029/2002JD 003296.

Estman, J. L., M. B. Coughenour, and R. A. Pielke Sr., 2001: Does grazing affect regional climate? *J. Hydrometeor.*, **2**, 243−253.

Ham, S., J.-W. Lee, and K. Yoshimura, 2016: Assessing future climate changes in the East Asian summer and winter monsoon using regional spectral model. *J. Meteor. Soc. Japan*, **94A**, 69−87.

Hawkins, E., and R. Sutton, 2011: The potential to narrow uncertainty in projections of regional precipitation change. *Climate Dyn.*, **37**, 407−418.

Hirai, M., T. Sakashita, H. Kitagawa, T. Tsuyuki, M. Hosaka, and M. Oh'izumi, 2007: Development and validation of a new land surface model for JMA's operational global model using the CEOP observation dataset. *J. Meteor. Soc. Japan*, **85A**, 1−24.

Hong, S.-Y., H.-M. H. Juang, and Q. Zhao, 1998: Implementation of prognostic cloud scheme for a regional spectral model. *Mon Wea. Rev.*, **126**, 2621−2639.

Hong, S.-Y., and J.-O. J. Lim, 2006: The WRF single–moment 6–class microphysics scheme (WSM6). *J. Korean Meteor. Soc.*, **42**, 129−151.

Hong, S.-Y., and H.-L. Pan, 1996: Nonlocal boundary layer vertical diffusion in a medium-range forecast model. *Mon. Wea. Rev.*, **124**, 2322−2339.

Hong, S.-Y., and H.-L. Pan, 1998: Convective trigger function for a mass-flux cumulus parameterization scheme. *Mon. Wea. Rev.*, **126**, 2599−2620.

Iacono, M. J., J. S. Delamere, E. J. Mlawer, M. W. Shephard, S. A. Clough, and W. D. Collins, 2008: Radiative forcing by long–lived greenhouse gases: Calculations with the AER radiative transfer models. *J. Geophys. Res.*, **113**, D13103.

Iizumi, T., M. Nishimori, K. Dairaku, S. A. Adachi, and M. Yokozawa, 2011: Evaluation and intercomparison of downscaled

daily precipitation indices over Japan in present-day climate: Strengths and weaknesses of dynamical and bias correction-type statistical downscaling methods. *J. Geophys. Res.*, **116**, doi:10.1029/2010JD014513.

Inatsu, M., T. Sato, T. J. Yamada, R. Kuno, S. Sugimoto, M. A. Farukh, Y. N. Pokhrel, and S. Kure, 2015: Multi-GCM by multi-RAM experiments for dynamical downscaling on summertime climate change in Hokkaido. *Atmos. Sci. Lett.*, **16**, 297−304, doi:10.1002/asl2.557.

IPCC, 2013: *Climate Change 2013: The Physical Science Basis. Contribution of Working Group I to the Fifth Assessment Report of the Intergovernmental Panel on Climate Change*. Stocker, T. F., D. Qin, G.-K. Plattner, M. Tignor, S. K. Allen, J. Boschung, A. Nauels, Y. Xia, V. Bex, and P. M. and Midgley, Eds., Cambridge University Press, Cambridge, UK and New York, USA, 1535 pp.

Ishizaki, N. N., I. Takayabu, M. Oh'izumi, H. Sasaki, K. Dairaku, S. Iizuka, F. Kimura, H. Kusaka, S. A. Adachi, K. Kurihara, K. Murazaki, and K. Tanaka, 2012: Improved performance of simulated Japanese climate with a multi-model ensemble. *J. Meteor. Soc. Japan*, **90**, 235−254.

Juang, H.-M. H., 2000: The NCEP mesoscale spectral model: The revised version of the nonhydrostatic regional spectral model. *Mon. Wea. Rev.*, **128**, 2329−2362.

Kato, T., 1995: A Box-Lagrangian rain-drop scheme. *J. Meteor. Soc. Japan*, **73**, 241−245.

Kain, J. S., 2004: The Kain-Fritsch convective parameterization: An update. *J. Appl. Meteor.*, **43**, 170−181.

Kitoh, A., and T. Uchiyama, 2006: Changes in onset and withdrawal of the East Asian summer rainy season by multi-model global warming experiments. *J. Meteor. Soc. Japan*, **84**, 247−258.

Kusaka, H., A. Suzuki-Parker, T. Aoyagi, S. A. Adachi, and Y. Yamagata, 2016: Assessment of RCM and urban scenarios uncertainties in the climate projections for August in the 2050s in Tokyo. *Climatic Change*, **137**, 427−438.

Mearns, L. O., R. Arritt, S. Biner, M. S. Bukovsky, S. McGinnis, S. Sain, D. Caya, J. Correlia Jr., D. Flory, W. Gutowski, E. S. Takle, R. Jones, R. Leung, W. Moufouma-Okia, L. McDaniel, A. M. B. Nunes, Y. Qian, J. Roads, L. Sloan, and M. Snyder, 2012: The North American regional climate change assessment program: Overview of phase I results. *Bull. Amer. Meteor. Soc.*, **93**, 1337−1362.

Mellor, G. L., and T. Yamada, 1982: Development of a turbulence closure model for geophysical fluid problems. *Rev. Geophys. Space Phys.*, **20**, 851−875.

Mizuta, R., O. Arakawa, T. Ose, S. Kusunoki, H. Endo, and A. Kitoh, 2014: Classification of CMIP5 future climate responses by the tropical sea surface temperature changes. *SOLA*, **10**, 167−171.

Nakanishi, M., and H. Niino, 2004: An improved Mellor–Yamada level-3 model with condensation physics: Its design and verification. *Bound.-Layer Meteor.*, **112**, 1−31.

Nakanishi, M., and H. Niino, 2006: An improved Mellor–Yamada level 3 model: Its numerical stability and application to a regional prediction of advecting fog. *Bound.-Layer Meteor.*, **119**, 397−407.

Nayak, S., and K. Dairaku, 2016: Future change in extreme precipitation intensities associated with temperature under SRES A1B scenario. *Hydro. Res. Lett.*, **10**, 139−144.

Nayak, S., K. Dairaku, I. Takayabu, A. Suzuki-Parker, and N. N. Ishizaki, 2017: Extreme precipitation linked to temperature over Japan: Current evaluation and projected changes with multi-model ensemble downscaling. *Climate Dyn.*, doi: 10.1007/s00382-017-3866-8.

Pielke, R. A., W. R. Cotton, R. L. Walko, C. J. Tremback, W. A. Lyons, L. D. Grasso, M. E. Nicholls, M. D. Moran, D. A. Wesley, T. J. Lee, and J. H. Copeland, 1992: A comprehensive meteorological modeling system: RAMS. *Meteor. Atmos. Phys.*, **49**, 69−91.

Rowell, D. P., 2005: A scenario of European climate change for the late twenty-first century: Seasonal means and interannual variability. *Climate Dyn.*, **25**, 837−849.

Rummukainen, M., B. Rockel, L. Bärring, J. H. Christensen, and M. Reckermann, 2015: Twenty-first-century challenges in regional climate modeling. *Bull. Amer. Meteor. Soc.*, doi: 10.1175/BAMS-D-14-00214.1.

Saito, K., T. Fujita, Y. Yamada, J. Ishida, Y. Kumagai, K. Aranami, S. Ohmori, R. Nagasawa, S. Kumagai, C. Muroi, T. Kato, H. Eito, and Y. Ymazaki, 2006: The operational JMA nonhydrostatic mesoscale model. *Mon. Wea. Rev.*, **134**, 1266−1298.

Skamarok, W. C., J. B. Klemp, J. Dudhia, D. O. Gill, D. M. Barker, M. G. Duda, X. Y. Huang, W. Wang, and J. G. Powers, 2008: A description of the Advanced Research WRF version 3. *NCAR Tech Note*, NCAR/TN-475+STR.

Sugimoto, S., R. Ito, K. Dairaku, H. Kawase, H. Sasaki, S. Watanabe, Y. Okada, S. Kawazoe, T. Yamazaki, and T. Sasai, 2018: Impact of spatial resolution on simulated consecutive dry days and near-surface temperature over the central mountains in Japan. *SOLA*, **14**, 46−51.

Takayabu, I., H. Kanamaru, K. Dairaku, R. Benestad, H. von Storch, and J. H. Christensen, 2016: Reconsidering the quality and utility of downscaling. *J. Meteor. Soc. Japan*, **94A**, 31−45.

Taylor, K. E., 2001: Summarizing multiple aspects of model performance in a single diagram. *J. Geophys. Res.*, **106**, 7183−7192.

Tewari, M., F. Chen, W. Wang, J. Dudhia, M. A. LeMone, K. Mitchell, M. Ek, G. Gayno, J. Wegiel, and R. H. Cuenca, 2004: Implementation and verification of the unified NOAH land surface model in the WRF model. *20th Conf. on Weather Analysis and Forecasting/16th Conf. on Numerical Weather Prediction*, pp. 11−15.

Tsunematsu, U., K. Dairaku, and J. Hirano, 2013: Future changes in summertime precipitation amounts associated with topography in the Japanese islands. *J. Geophys. Res. Atmos.*, **118**, 4142−4153.

van der Linden, P., and J. F. B. Mitchell, 2009: *ENSEMBLES: climate change and its impacts: summary of research and results from the ENSEMBLES project*. Met Office Hadley Centre, UK, 160 pp.

von Storch, H., and F. W. Zwiers, 1999: *Statistical Analysis in Climate Research*. Cambridge University Press, Cambridge, UK, 496 pp.

Walko, R. L., C. J. Tremback, R. A. Pielke, and W. R. Cotton, 1995: An interactive nesting algorithm f or stretched grids and variable nesting ratios. *J. Appl. Meteor.*, **34**, 994−999.

Xie, S.-P., C. Deser, G. A. Vecchi, J. Ma, H. Teng, and A. T. Wittenberg, 2010: Global warming pattern formation: Sea surface temperature and rainfall. *J. Climate*, **23**, 966−986.

Yamada, Y., 2003: Cloud microphysics. The JMA nonhydrostatic model. *Japan Meteorological Agency Annual Report*, **49**, 52−76 (in Japanese).

Manuscript received 2 May 2018, accepted 19 June 2018
SOLA: *https://www.jstage.jst.go.jp/browse/sola/*